BALLOONING MODES IN AN $L = 2$ HELIOTRON/TORSATRON SYSTEM

N. Nakajima, J. Chen*, and M. Okamoto

NIFS, Japan
** Graduate University For Advanced Studies, Japan*

1. Introduction

In the heliotron/torsatron system with the polarity of the helical coils $L = 2$ and the toroidal field period of them $M = 10$, it has been shown that 1) the change of the local magnetic shear due to a large Shafranov shift is essentially axisymmetric, i.e., toroidicity dominant, leading to disappearance of the local shear outside the torus even in the stellarator-like global magnetic shear region [1], 2) the local magnetic curvature consists of both parts due to toroidicity and helicity of the helical coils [2]. In the 3D equilibria, the eigenvalues of ballooning modes in the local theory ω^2 are functions with respect to the labels of the flux surface ψ and the magnetic field line α, and the radial wave number θ_k: $\omega^2 = \omega^2(\psi, \theta_k, \alpha,)$. Since ω^2 has no α-dependence in axisymmetric systems, the stronger the α-dependence of ω^2 mainly coming from the local magnetic curvature is, the more significant the 3D properties of ω^2 are. The followings have been found in the local theory [2]: 1) In Mercier unstable equilibria, there coexist two types of topological level surfaces of $\omega^2(< 0)$ in (ψ,θ_k, α) space. One is a tokamak-like, topologically cylindrical level surface with the axis in α direction, and the other is topologically spheroidal level surface inherent in 3D systems, 2) In Mercier stable equilibria, only topologically spheroidal level surface exists. The global structure of the pressure-driven modes in 3D real space has been conjectured [2]: 1) Modes corresponding to ones with topologically cylindrical level surface of ω^2 in the local analysis are poloidally localized tokamak-like ballooning modes or interchange modes. 2) Modes corresponding to ones with topologically spheroidal level surface of ω^2 in the local analysis are ballooning modes inherent in 3D systems with quite high poloidal and toroidal mode numbers and localizing in both poloidal and toroidal directions.

The purposes of this paper are 1) to prove above conjecture of the local analysis, and 2) to clarify the inherent properties of pressure-driven modes in 3D systems through the global analysis of Mercier unstable equilibria.

2. Properties of equilibria

As is mentioned above, 3D properties of ω^2 in the local analysis mainly stems from the properties of the local magnetic curvature consisting of both toroidicity and helicity parts. Therefore, two types of Mercier unstable equilibria are adopted in order to examine the competitive or synergetic effects of toroidicity and helicity on pressure-driven modes. One is a toroidicity-dominant equilibrium with a peaked pressure profile (β on axis is 5.9 %) under the flux conserving condition, and the other is a helicity-dominant equilibrium with a broad pressure profile (β on axis is 4 %) under the currentless condition. Both equilibria have the same boundary, and the latter is exactly same as one in Ref. 2. In Figs. 1 - (a) and 1 - (b), the contours of driving term $dP/d\psi\kappa^n$ are shown for both equilibria. In the case of toroidicity-

dominant equilibrium, asymmetry of the locally bad magnetic curvature region with $dP/d\psi\kappa^n$ (> 0) between inside and outside the torus is clear as shown in Fig. 1 - (a). In contrast with it, as shown in Fig. 1 - (b), symmetry of the locally bad curvature region fairly exists between the inner and the outer side of the torus in the helicity-dominant equilibrium. Note that the local badness of the magnetic curvature in the helicity-dominant equilibrium is stronger inside the torus than that outside the torus.

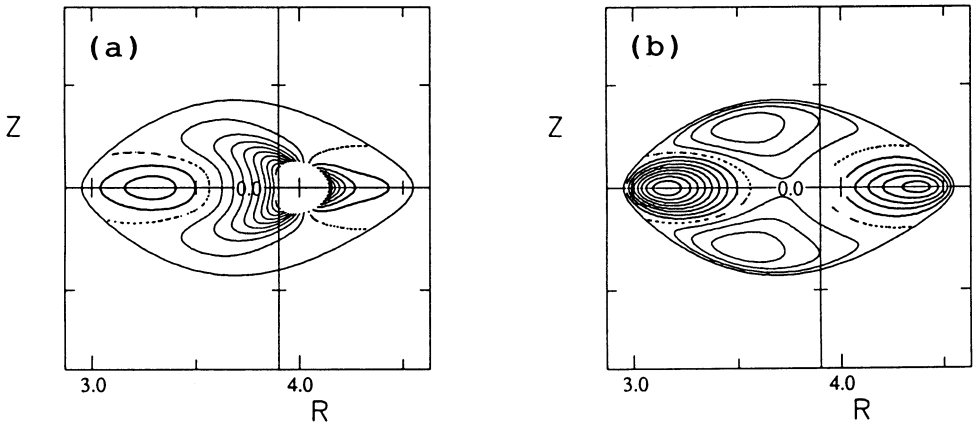

Fig. 1. Contours of $dP/d\psi\kappa^n$ on the horizontally elongated poloidal cross section for (a) toroidicity-dominant equilibrium, and (b) helicity-dominant equilibrium. Thick and thin curves indicate positive (bad) and negative (good) region, respectively.

3. Global analysis in the toroidicity-dominant equilibrium

The global analysis has been done by using CAS3D code [3]. Let n and M be the typical toroidal mode number of the perturbation and the toroidal field period of the equilibrium, respectively. For low toroidal mode number with $n < M$, interchange modes easily feeling the averaged magnetic curvature occur. For medium toroidal mode number with $n \sim M$, modes become to feel the local structure of the magnetic curvature, in which effects of toroidicity are dominant in this equilibrium as shown in Fig. 1-(a). Thus, poloidally localized tokamak-like ballooning modes occur as shown in Fig. 2. - (a), where the radial distribution of the Fourier components of the normal displacement vector $\vec{\xi} \cdot \nabla\psi$ is drawn. There are three groups of the Fourier modes with different toroidal mode numbers specified in the figure, and each group consists of the Fourier modes with different poloidal mode numbers through poloidal mode coupling. In this case, the group with $n = -21$ is dominant and the toroidal mode coupling is weak, leading to the poloidal localized tokamak-like ballooning mode. For fairly high toroidal mode number with $n \gg M$, modes can distinguish the fine structure of the magnetic curvature, resulting in the situation that ballooning modes inherent in 3D systems occur which have both strong poloidal and toroidal mode couplings and localize in both poloidal and toroidal directions. One example is shown in Fig. 2 - (b) where eight groups exist with different toroidal mode numbers and a comparable magnitude, which leads to both poloidally and toroidally localized ballooning structure. The contours of the perturbed pressure $\tilde{P} = -\nabla P \cdot \vec{\xi}$ corresponding to Fig. 2 - (b) on two poloidal cross sections are shown in Fig. 3 - (a) and 3 - (b). The outer side of the torus at the horizontally (vertically) elongated poloidal cross section is locally bad (good) curvature region, thus, the perturbed pressure existing on the outer side of

the torus at the horizontally elongated poloidal cross section disappears on the outer side of the torus at the vertically elongated poloidal cross section.

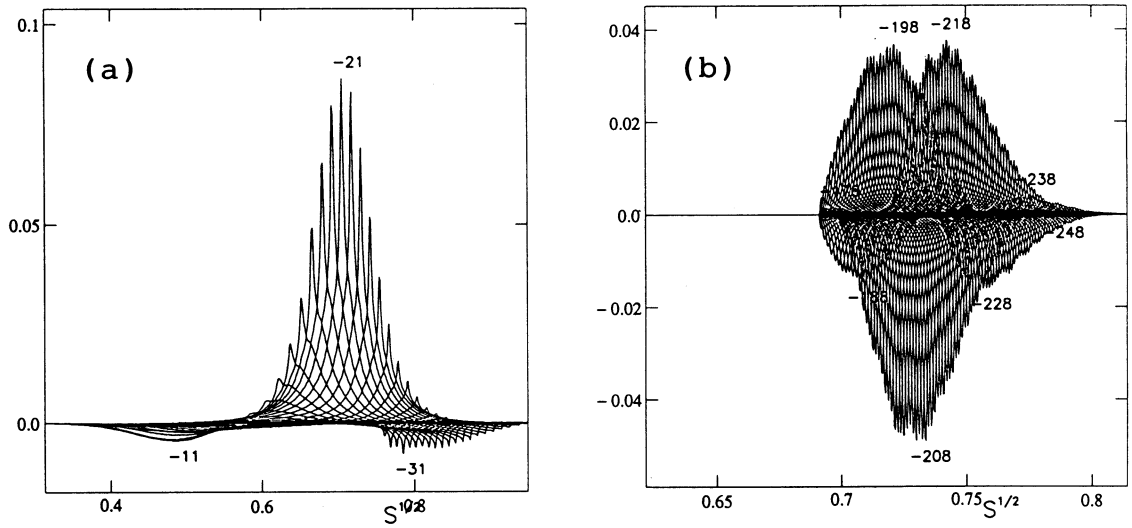

Fig. 2. Fourier components of $\vec{\xi}\cdot\nabla\psi$ vs. normalized minor radius $s^{1/2}$ for (a) medium toroidal mode numbers, and (b) fairly high toroidal mode numbers. Figures denote the toroidal mode numbers for each group.

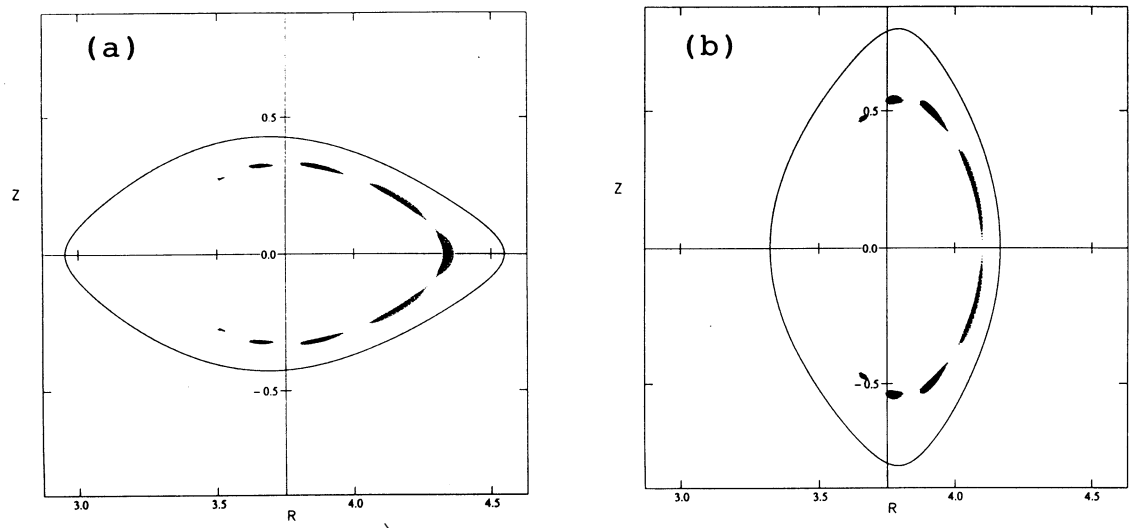

Fig. 3. Contours of $\tilde{P} = -\nabla P\cdot\vec{\xi}$ corresponding to Fig. 2. - (b) on (a) horizontally and (b) vertically elongated poloidal cross sections.

4. Global analysis in the helicity-dominant equilibrium

For low toroidal mode number with $n < M$, interchange modes occur. For medium toroidal mode number with $n \sim M$, interchange modes still occur in contrast with the case in the toroidicity-dominant equilibrium, the reason of which stems from the fact that effects of helicity on the local magnetic curvature are stronger than ones of toroidicity as shown in Fig. 1 - (b). Although toroidal mode coupling of interchange modes becomes stronger with the toroidal mode number, poloidally localized tokamak-like ballooning modes do not appear in the helicity-dominant Mercier unstable equilibria. Moreover, as shown in Fig. 4, interchange modes with $n < M$ or $n \sim M$ more localize on the inner side of the torus, which is consistent with the distribution of the locally bad magnetic curvature between inside and

outside the torus in Fig. 1 - (b). In Fig. 4. - (a), the radial distribution of the Fourier components of the normal displacement vector $\vec{\xi}\cdot\nabla\psi$ is drawn, where the origin of the poloidal angle is shifted from the outer side to the inner side of the torus in order to clarify the poloidal localization. The contours of the perturbed pressure $\tilde{P} = -\nabla P\cdot\vec{\xi}$ corresponding to Fig. 4. - (a) are shown in Fig. 4. - (b).

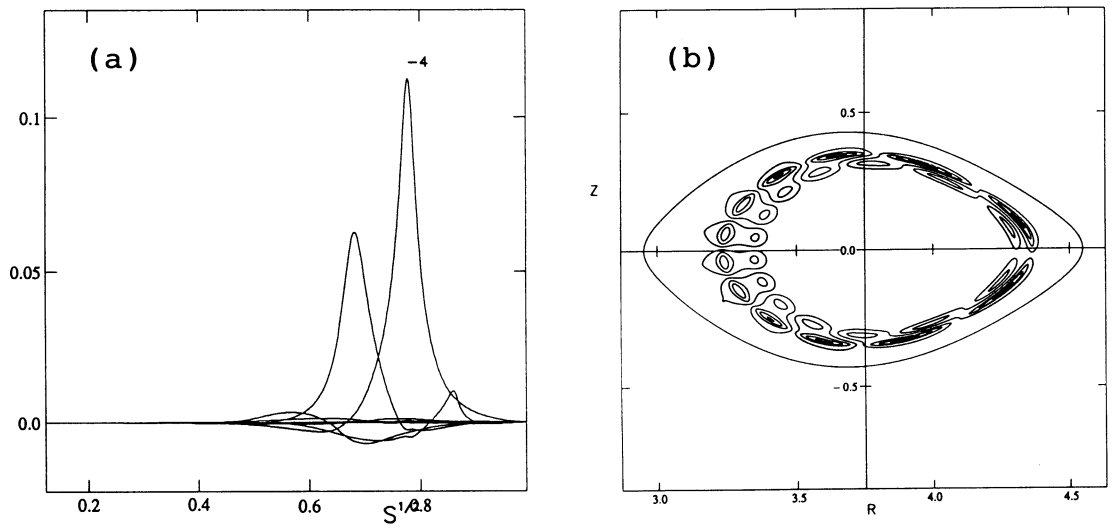

Fig. 4. (a) Fourier components of $\vec{\xi}\cdot\nabla\psi$ vs. normalized minor radius $s^{1/2}$ for the low toroidal mode number $n = -4$, and (b) corresponding contours of $\tilde{P} = -\nabla P\cdot\vec{\xi}$ on horizontally elongated poloidal cross section.

5. Conclusions

The characteristics of the pressure-driven modes in Mercier unstable $L = 2/M = 10$ heliotron/torsatron MHD equilibria dramatically change according to both the competitive relation between toroidicity and helicity in the local magnetic curvature and the great and small relation between the typical toroidal mode number of the perturbation n and the toroidal field period of the equilibrium M. In the toroidicity-dominant Mercier unstable equilibria, the pressure-driven modes change from interchange modes for $n < M$, to poloidally localized tokamak-like ballooning modes with weak toroidal mode coupling for $n \sim M$, and finally to poloidally and toroidally localized ballooning modes purely inherent in 3D systems with both strong poloidal and toroidal mode couplings for $n \gg M$. In contrast with it, in the helicity-dominant Mercier unstable equilibria, the pressure-driven modes change from interchange modes localizing on the inner side of the torus for $n < M$ or $n \sim M$, directly to poloidally and toroidally localized ballooning modes purely inherent in 3D systems with both strong poloidal and toroidal mode couplings for $n \gg M$. The global analysis in Mercier stable equilibria, the continuous unstable spectrum, and stabilizing effects due to the finite Larmor radius, will be reported elsewhere.

References

[1] N. Nakajima: Phys. Plasmas **3**, 4545 (1997).
[2] N. Nakajima: Phys. Plasmas **3**, 4556 (1997).
[3] C. Schwab: Phys. Fluids B **5**, 3195 (1993).